Dislocation glide in model Ni(Al) solid solutions by molecular dynamics

E. Rodary,[1] D. Rodney,[2] L. Proville,[1] Y. Bréchet,[3] and G. Martin[1]
[1]*Service de Recherches de Métallurgie Physique, CEA-Saclay, 91191 Gif sur Yvette, France*
[2]*GPM2/ENSPG, Domaine Universitaire BP 46, 38402 St Martin d'Hères Cedex, France*
[3]*LTPCM/ENSEEG, Domaine Universitaire BP 75, 38402 St Martin d'Hères Cedex, France*
(Received 23 March 2004; published 31 August 2004)

The glide of an edge dislocation, in a random solid solution, Ni (1 to 8 at % Al), is simulated by molecular dynamics (MD). An embedded atom method potential has been optimized to reproduce the relevant properties of the face centered cubic solid solution and of the $L1_2$ Ni_3Al phase. Glide is studied at fixed temperature and applied stress. Three parameters are found to be necessary to describe the rate of shear as a function of applied shear stress: σ_s is the static threshold stress, below which the glide distance of the dislocation is not sufficient to insure sustained shearing; σ_d is the dynamical threshold stress, which reflects the friction of the pinning potential on the moving dislocation; B is the friction coefficient, which relates the effective stress $(\sigma-\sigma_d)$ to the glide velocity. We also find that the obstacles are made of specific configurations of the Al atoms, which are brought in positions of strong mutual repulsion in course of the glide process. The solute-solute short range repulsion, rather than the usually assumed dislocation-solute interaction, is thus argued to be the main mechanism responsible for chemical hardening in the present concentrated random solid solution. The use of the above results in the frame of multi-scale modeling is exemplified.

DOI: 10.1103/PhysRevB.70.054111 PACS number(s): 62.20.Fe

I. INTRODUCTION

While the elastic theory is well suited for most problems related to dislocations, atomic scale modeling is unique for describing the core of dislocations [e.g., Ref. 1], the effect of electronic structure on the latter (materials chemistry),[2] and ultimately the selection of the glide systems.[3] Also unexpected features are revealed by atomic scale modeling, when studying the interaction of dislocations with defect clusters (e.g., self-interstitials,[4–6] stacking fault tetrahedra,[7] cavities and precipitates[8]), or dislocation nucleation at locations of strong stress concentration, e.g., in nano-indentation,[9,10] at crack tips[11–13] or in small confined devices.[14]

Here we address the question of dislocation glide in concentrated solid solutions, with Ni(Al) as a prototype. The classical scheme for describing hardening in random solid solutions, is inherited from that of precipitate- and of dilute solution- hardening:[15–17] The glide of the dislocation line proceeds under the combined effect of the external stress, the line tension and the dislocation -precipitate or -solute atom interaction. In the case of a concentrated solid solution, the potential energy surface, along which the dislocation moves, results from the superposition of two contributions: A far field one, with undulations of weak amplitude, resulting from the long range strain field of the solute atom population, and a short range contribution due to the solute atoms close to the dislocation. The equilibrium shape of a dislocation in such a strain field results from the balance between the line tension of the dislocation (in a medium with elastic constants which depend on the solute content), and the interaction energy of the dislocation with the strain field of the solute population. The glide of the dislocation follows a complex path, made of obstacle unpinning events, which trigger cascades of crossings of lower potential energy barriers. A detailed simulation of such a process at zero and finite temperatures can be found in Refs. 18–21 with application to internal friction in solid solutions.[22] Note that, in such models, when calculating the potential energy surface along which the dislocation movement proceeds, the position of the solute atoms is taken as fixed (frozen), unaffected by the glide process.

Here we want to explore whether this classical scheme, which is quite efficient for dilute random solid solutions or for precipitates, is realistic in the case of more concentrated solid solutions, i.e., whether this scheme is appropriate for what is known as *chemical hardening*. We consider here random solid solutions; the effect of short range order is beyond the scope of the present paper. For this purpose, we simulate the glide process of a dislocation at the atomic scale and study the glide distance as a function of time under a broad range of applied stresses, and for a range of compositions.

In the following, we first develop an energy model for Ni(Al) solid solutions and give some details on the molecular dynamics technique we use to simulate the glide of an edge dislocation (Sec. II). We then describe the shear rate observed in our simulations, as a function of the applied stress, for solute contents ranging from 1 to 8 at %, at 300 K (Sec. III). Several "*in situ*" observations show that dislocation pinning results from specific configurations of the Al atoms which are brought in positions of strong mutual repulsion in course of the glide process. This is the main finding of this study. In the discussion section, we outline the possible strategies to incorporate the present findings into a micromechanical model.

II. ENERGY MODEL AND METHODOLOGY

Dislocation glide is simulated by molecular dynamics (MD) at constant temperature and applied stress in a way similar to that described in Refs. 4 and 5. Following the pioneering work by Daw and Baskes,[11,23] we employ an em-

TABLE I. Parameter values chosen for the EAM potential (see text).

c_1(eV)	2.7277	c_4(keV nm^{-3})	87.5715	s_{AL}	3.8804
c_2(nm^{-1})	16.765	r_{cut}^{NiAl}(nm)	0.46168	g_{AL}(meV nm^3)	−9.5130
c_3(nm)	0.19915	r_{inf}(nm)	0.15	g_{Ni}(meV nm^3)	6.0178

bedded atom method (EAM) interatomic potential which provides a good compromise between the realism of dislocation simulation and the computational load necessary to handle a system large enough to keep at least part of the complexity of the real alloy and to minimize the influence of the boundary conditions. In order to simulate dislocation glide in a Ni-rich Ni-Al solid solution, the energy model had to be based on a Ni potential adapted to such simulations. The Ni-Al potentials published in the literature (e.g., Refs. 24 and 25) use Ni potentials with stacking fault energies too low to simulate realistic dislocation dissociations. We thus had to optimize a new one. The requirement for this potential is to provide a reasonable description of the elastic properties and stacking fault energies and of their dependence with composition.

A. Energy model for the Ni(Al) solid solution

In the framework of the EAM, the total energy of the alloy is additive.[24,26] The energy of each atom is the sum of two terms: A repulsive part, written as a sum of pairwise interactions $\Phi_{\alpha\beta}$ (with α,β=Ni, Al), and an embedding energy, $F_\alpha[\rho(r)]$, which depends only on the nature, α, of the embedded atom and on the electronic density, $\rho(r)$, at the position, r, of that atom. The electronic density is the sum of single atom functions: $\rho(r)=\Sigma_\beta\rho_\beta(r)$. As a consequence, the EAM model for an alloy implies 7 functions, 6 of which describe the pure elements ($\Phi_{\alpha\alpha}, F_\alpha, \rho_\alpha, \alpha$=Ni, Al), and only one, $\Phi_{\alpha\beta}$, $\alpha\neq\beta$, is specific to the alloy. For the sake of simplicity, we started from homo-atomic functions taken from the literature and constructed only Φ_{NiAl}.

For pure nickel we chose the potential developed by Angelo *et al.* which has proved to be well adapted to the atomic scale simulation of dislocations.[5,26] In particular, the dissociation width of the edge dislocation is quantitatively well reproduced by this potential. For pure aluminum we chose the potential proposed by Voter and Chen,[24] which has the drawback of yielding a low stacking fault energy (compared, e.g., to the potential of Ercolessi *et al.*[27]), but has the advantage of being written in the very same functional form as that for Ni, which makes the optimization procedure, to be described below, more tractable.

As for Φ_{NiAl}, we keep the form used for pure metals (first term in the equation below, using Angelo's notation[26]) augmented by a short distance repulsive term (last term):

$$\Phi_{NiAl}(r) = c_1[\exp(-2c_2(r-c_3)) - c_2(r-c_3)] \times\exp(1/(r-r_{cut}^{NiAl})) + c_4(r_{inf}-r)^3H(r_{inf}-r). \quad (1)$$

In Eq. (1), $H(x)$=0, or 1, respectively, for $x<0$ or $\geqslant 0$. The last term in the right-hand side (RHS) of Eq. 1, of the same form as proposed by Ludwig and Gumbsch[25] was found useful in view of the large size effect of Al in Ni and of the existence of very large strains in the dislocation core region. The range, r_{inf}, was not optimized but fixed to 0.15 nm.

In order to give more flexibility to the optimization of the potential, we introduced three more parameters in the homo-atomic functions, in a way not to alter the quality of the fit to the properties of the pure metals (see Ref. 24 for more details). Keeping Voter's notation, these are: s_{Al}, which scales the electronic density function of Al, g_{Al} and g_{Ni}, which shift the repulsive and embedding energy contributions of pure Al and Ni while, keeping the balance constant.

These eight parameters were optimized by an iterative procedure: First, a simulated annealing technique is used to adjust the parameters with a merit function written as the sum of the squares of the relative deviations of material properties, calculated with the potential, from their values known experimentally. These properties are evaluated from a rigid lattice model and are relative to the $L1_2$ Ni_3Al compound (lattice parameter, cohesive energy, C_{11}, C_{12}, C_{44}, and C'_{44} elastic constants) and to the solid solution (the lattice parameter with 7.3 and 10.5 at % Al, for which precise measurements are available[28]); when modeling the solid solution, local order, as measured in Ref. 28 is taken into account. Second, the potential so obtained is used to simulate the fully relaxed solid solution at finite temperature, using a Monte Carlo (MC) technique. The volume, atomic positions, and local chemical order are explored using Metropolis algorithm, varying the volume, displacing atoms and permuting the latter, with respective probabilities of 1/8, 3/4, and 1/8. The parameters are accordingly adapted, in order to improve the realism of the simulation. The values of the parameters obtained by this procedure are given in Table I.

B. Assessment of the energy model

The model for pure nickel yields the correct value of the lattice parameter, a reasonable shear modulus (within 1% of the experimental data) and acceptable stacking fault energy (too small by 28%, when compared to the mean value of the scattered existing experimental data). When 1 to 8 at % Al are added in a fully random manner and the solid solution is simulated by the MC technique, we find, in agreement with existing experimental data, a roughly linear increase of the lattice parameter and a decrease of the shear modulus and of the stacking fault energy. The quantitative assessment is shown in Table II.

The melting temperature is of the right order of magnitude. On the other hand, the predicted solubility limit is too small by one order of magnitude. In the following, dislocation glide is studied by MD at temperatures and time scales

TABLE II. Properties of (a) the Ni(Al) solid solution and (b) the Ni_3Al γ' phase, as given by the EAM potential compared to experimental values. In (a), c, a, μ, E_{sf}, T_m, c_{max} stand, respectively, for the Al concentration, the lattice constant, the shear modulus, the stacking fault energy, the melting temperature and the solubility limit at 1500 K. In (b), E_0, stands for the cohesive energy and the C_{ij}'s for the elastic constants with the classical notation.

Ni(Al) Solid Solution[a]	This Model	Experiment
$\partial a/a\ \partial c(\text{Al at\%})^{-1}$	~ 0.01	~ 0.0068[a]
$\partial\mu/\mu\partial c(\text{Al at\%})^{-1}$	~ -0.02	~ -0.01[b]
$\partial E_{sf}/E_{sf}\partial c(\text{Al at\%})^{-1}$	~ -0.125	~ -0.017[c]
T_m(K)	1750 ± 200	$1725 \rightarrow 1700$[d]
c_{max}(1500 K)(Al at%)	~ 1	10[d]
Ni_3Al γ' phase[b]	This Model	Experiment
a(nm)	0.3571	0.3567[e]
E_0(eV)	−4.52	−4.57[f]
C_{11}(GPa)	231	223[e]
C'_{44}(GPa)	70	67[e]
C_{12}(GPa)	131	148[e]
C_{44}(GPa)	111	125[e]

[a]Reference 28.
[b]Reference 29.
[c]Reference 30.
[d]Reference 31.
[e]Reference 32.
[f]Reference 33.

where thermally activated atomic diffusion cannot proceed. As a consequence, highly supersaturated solutions can be handled without problem. However, the underestimate of the solubility limit by our potential is a consequence of too large ordering energies, which may result in an overestimate of the short range repulsion among Al atoms. This, we expect, might reinforce the chemical hardening we are studying.

C. Technical details

The computation cell we use is depicted in Fig. 1. The X, Y, Z directions are parallel, respectively, to $[110]$, $[\bar{1}12]$, $[1\bar{1}1]$. The $(1\bar{1}1)$ glide plane is perpendicular to Z. Periodic boundary conditions prevail in the X and Y directions, while the movements of the atoms in the upper and lower free surfaces parallel to the glide plane are confined in the planes $\pm Z_{max}$. The effect of imposing periodic boundary conditions in the X direction has been discussed in Ref. 5.

A typical simulation proceeds as follows. Solute and solvent atoms are first located at random on the lattice, with the appropriate concentration. The precise dimensions of the box are adjusted in order to match the temperature and composition dependence of the lattice parameter of the random solid solution. The positions of the atoms are then set according to the elastic theory of dislocations, the edge dislocation being placed in the center of the box. The configuration so obtained is then relaxed, using a conjugate gradient routine, which

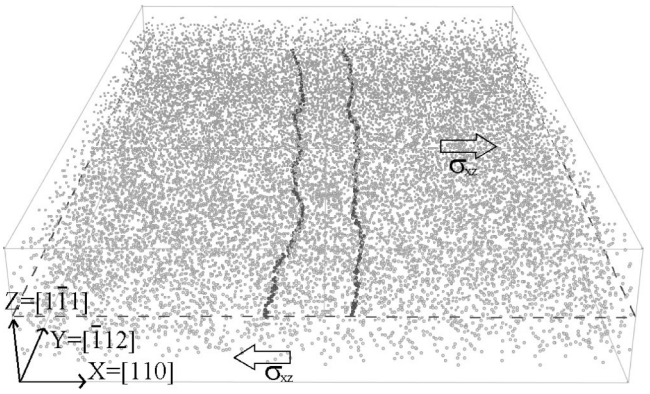

FIG. 1. Computational cell: The dislocation has decomposed into two Shockley partials in its glide plane (dashed line); atoms in the partial dislocation cores are shown, as well as the Al atoms of the solid solution $L_x=30$ nm, $L_y=43.12$ nm, $L_z=7.32$ nm. This cell comprises 867 000 atoms.

permits the dissociation of the dislocation. Initial velocities are taken from a Maxwell distribution and the MD simulation is started. Time integration is performed using Verlet's algorithm with a time step of 2.10^{-15} s. Temperature is maintained at a constant value by rescaling the atomic velocities every 10^2 time steps. After thermalization, the external stress is applied, i.e., a constant force, parallel to the glide direction, is added to each atom in the outer Z surfaces parallel to the glide plane. The intensity of the force is proportional to the inverse of the number of atoms in the plane, in order to make sure the force per unit area is the same (with opposite sign) in the upper and lower surfaces.

A standard method to identify atoms in dislocation cores in pure metals is to select the ones with highest energies.[12,13] In the present simulations, since the energy per atom is much contrasted in the solid solution, the energy scale is of no help. We rather identify the atoms in the dislocation cores as the ones having an environment, which exhibits neither a face centered cubic-, nor a hexagonal closed packed structure.[5]

The optimum size of the computational cell is a compromise between the duration of the computations, and the realism of the simulations. We mainly worked with a box containing 232 320 atoms. Some studies implied up to 867 600 atoms. The exact values of the box dimensions are adjusted in order to account for the dependence of the lattice parameter on temperature and composition. Several box widths L_y, in the Y direction (see Fig. 1) along the dislocation line, ranging from $L_y=8.6$ to 43.12 nm have been probed. Most simulations were performed with a box width of 17.2 and 21.56 nm. More details on the dependence of dislocation behavior on the value of L_y are given in Sec. III C. Several box lengths in the glide direction (direction X in Fig. 1) have been probed, ranging from 10 to 30.1 nm. For 15 nm and more, the dissociation width of the dislocation is almost insensitive to the length of the box. The interaction of the dislocation with its periodic images is screened by the interaction with the solute atoms. As for the thickness in the Z direction, we found 10 nm to be sufficient to screen the effect of the two-dimensional dynamics imposed to the atoms at the free surfaces.

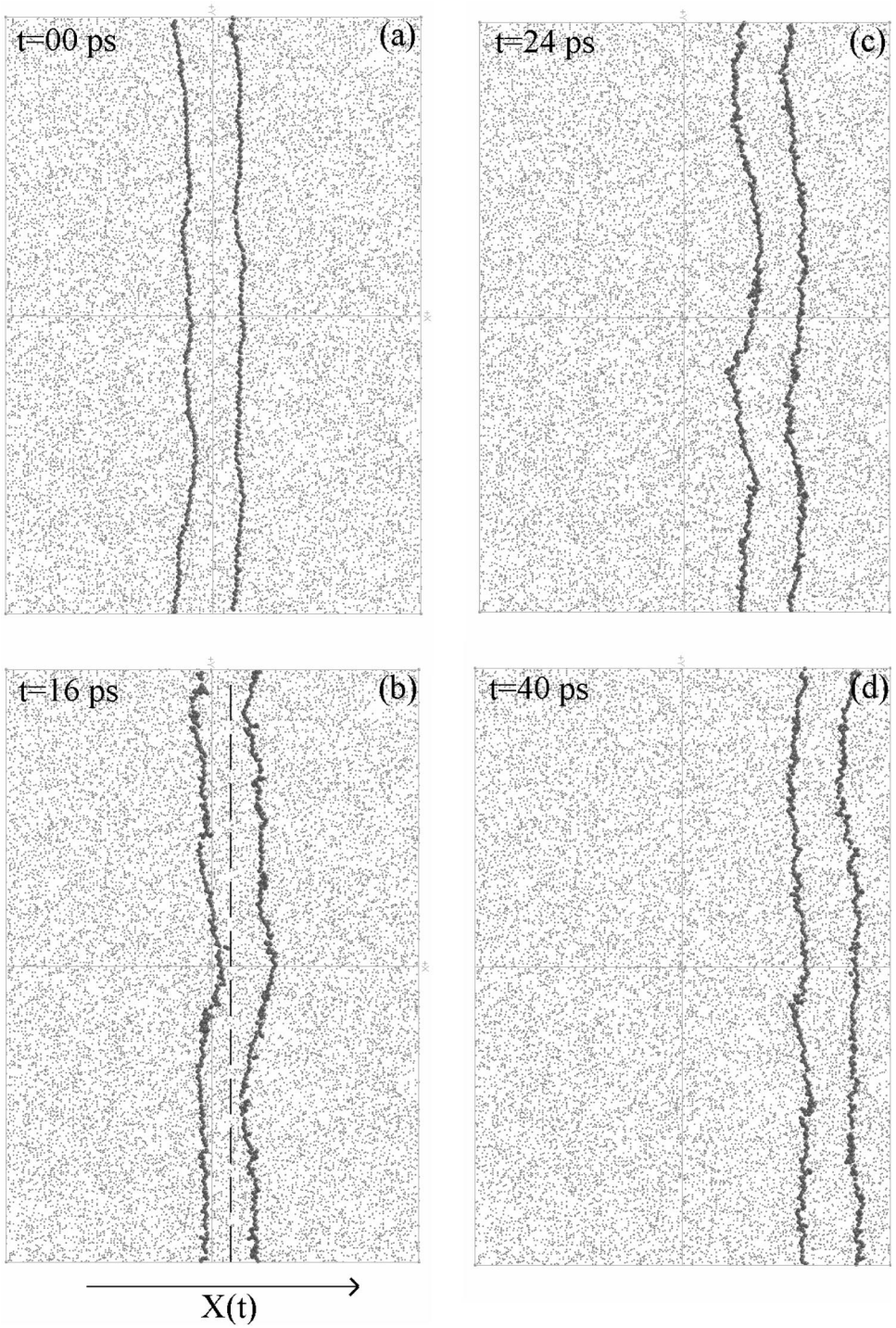

FIG. 2. Edge dislocation gliding in a 3 at % Al random solid solution, under 70 MPa at increasing times. The computational cell is the same as in Fig. 1, as seen along the $[\bar{1}11]$ direction. The arrow defines the position of the dislocation.

Figure 2 gives a typical image of the dissociated dislocation, together with the Al atoms, at successive steps of the glide process in the $(\bar{1}11)$ plane. In what follows, the position of the dislocation as a function of time, $X(t)$, will be extensively used. The latter is defined as the coordinate, along the glide direction, of the median of the staking fault ribbon; it is monitored every 2 *ps* (see Fig. 2).

III. DISLOCATION GLIDE VELOCITY AND SHEAR RATE

The quantity physically relevant to be extracted from the simulations is the dislocation velocity. The quantity of interest for macroscopic plasticity is the shear rate. It is related to the dislocation velocity via Orowan's equation: the shear rate, $\dot{\gamma}$ is proportional to the dislocation- velocity, V, and density, ρ_d: $\dot{\gamma}=\rho_d bV$, with b, the Burgers vector. In the simulations, the dislocation density is $1/hL$, with h and L, respectively, for the thickness (Z direction) and the length (X direction) of the computational cell. Since h and L are small, ρ_d is large (of the order of $5\ 10^{15}\ \mathrm{m}^{-2}$), and Orowan's equation would give very large shear rates although the velocity of individual dislocation segments is reasonable. In addition, for macroscopic shear to be observed, the dislocation seg-

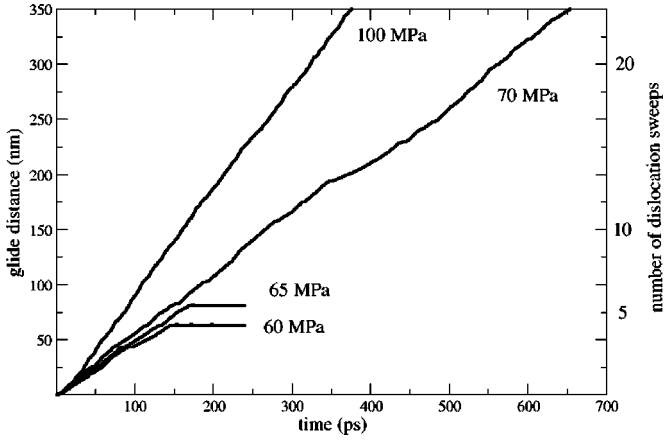

FIG. 3. Mean position of the dislocation, as a function of time, in a random 3% Al solid solution at 300 K with four distinct values of the applied stress: 60, 65, 70, and 100 MPa.

ment must glide on a distance large enough to promote the critical bending for unpinning from the forest dislocations. This latter process might be sensitive to the value of L_y (Fig. 1) which imposes the periodicity of the atomic configuration along the dislocation line. This point is discussed at the end of the present section. Before, we first describe our results on the dislocation glide velocity and the associated shear rate.

A. Dislocation glide velocity

All results given in the present section were obtained in *random solid solutions*, with $L_y = 17.2$ nm. The dependence of the results on this parameter is discussed in Sec. III C. Under a given applied stress, the dislocation glides in a more or less smooth manner. Figure 3 illustrates typical behaviors as observed in a solution with 3 at % Al, at 300 K, for four distinct values of the applied stress.

As can be seen, for an applied stress of 100 MPa, the dislocation glides for 300 nm within about 375 ps. The mean glide velocity (~ 0.8 nm.ps^{-1}) is thus well below the sound velocity ($C_s \sim 2$ nm.ps^{-1}). Notice that the glide distance of 300 nm is 20 times the length of the cell: The upper half of the cell has thus been shifted by 20 Burgers vectors with respect to the lower half. Each shift by one Burgers vector creates a new configuration of the Al atoms across the glide plane. To a first approximation, since we deal here with *random* solid solutions, we may consider that the sequence of configurations so produced is representative of the configurations one single dislocation would explore on gliding a distance of 300 nm.

For an applied stress of 70 MPa, the dislocation still glides for 300 nm, but with a lower mean velocity ($\sim 0.1\ C_s$), and in a much less smooth manner. For 65 MPa, the glide stops, for at least 50 ps, after about 5 sweeps of the cell. The delay of 50 ps, we use, is long enough for the sound to travel more than 5 times the length of the dislocation in the cell.

For an applied stress of 60 MPa, the glide is stopped in the course of the fourth sweep. At still lower an applied stress (<45 MPa), no glide is observed at all (at least within 50 ps). Some glide would probably be observed if very long simulations were performed. In a preliminary study, we found a large scatter of the time to wait to observe some glide, which prevented us from doing an extensive study of this lower stress threshold.

The latter threshold of 45 MPa, which depends on the duration of observation, corresponds to the onset stress for micro-creep, not to be confused with the yield stress. Indeed, for macroscopic shear to proceed, the dislocation segment must glide on a distance large enough to promote the critical bending for unpinning from the forest dislocations. In order to stay on the conservative side, we chose a minimum glide distance of 300 nm (corresponding to a dislocation density $\sim 2.8\ 10^{12}$ m^{-2}). With such a criterion, the *shear rate* is zero up to a minimum applied stress, which we name hereafter the *static* threshold stress, σ_s. From Fig. 3, e.g., in Ni 3 at % Al at 300 K, we find 65 MPa $< \sigma_s <$ 70 MPa.

B. Shear rate

Because of the boundary conditions imposed in the Z direction, the thickness h of the box is a constant and the shear rate of the computational cell scales with the dislocation velocity with a constant, b/hL. For that reason, in the following, we skip this transparent b/hL factor and define the effective dislocation velocity as the velocity the dislocation should have in order to account for the shear rate. Above the static threshold stress, the effective dislocation velocity is identical to the velocity measured in the simulation. Below the *static* threshold stress, although at the scale of the simulation, the dislocation can travel some distance, this distance is too small to allow for unpinning from the forest dislocations and to contribute significantly to the macroscopic strain (it would rather give rise to recoverable microplasticity): In this situation the effective dislocation velocity is zero.

Figure 4 shows the (effective) dislocation velocity, as a function of the applied stress, as observed in Ni(Al) random solid solutions with increasing Al contents (3, 5, 8 at%); pure Ni is shown for the sake of comparison. For very high values of the applied stress, the saturation of the dislocation velocity shows up. At intermediate stress values, a viscous regime is observed: The velocity is a linear function of the applied stress, with a friction coefficient (per unit length) B. Below the static threshold stress σ_s, the effective velocity drops to zero. The linear portion of the velocity versus stress curve extrapolates to zero velocity at the *dynamical* threshold stress σ_d. In the stress range of practical interest (i.e., before saturation), the effective dislocation velocity is thus defined by three parameters:

$$V = 0 \text{ if } \sigma < \sigma_s; \quad V = (\sigma - \sigma_d) b/B \text{ if } \sigma_s < \sigma, \quad \text{as long as } V \ll C_s. \tag{2}$$

In Eq. (2), σ_s, σ_d, and B are composition and temperature dependent.

The three parameters are found to increase linearly with the composition (Fig. 5): Starting from pure Ni where $\sigma_s = \sigma_d = 5$ MPa and $B = 11\ 10^{-6}$ Pa.s, the static threshold stress increases by ~ 25 MPa/at% Al, the dynamical one by ~ 15 MPa/at% and the friction by $\sim 2\ 10^{-6}$ Pa.s/at%, at

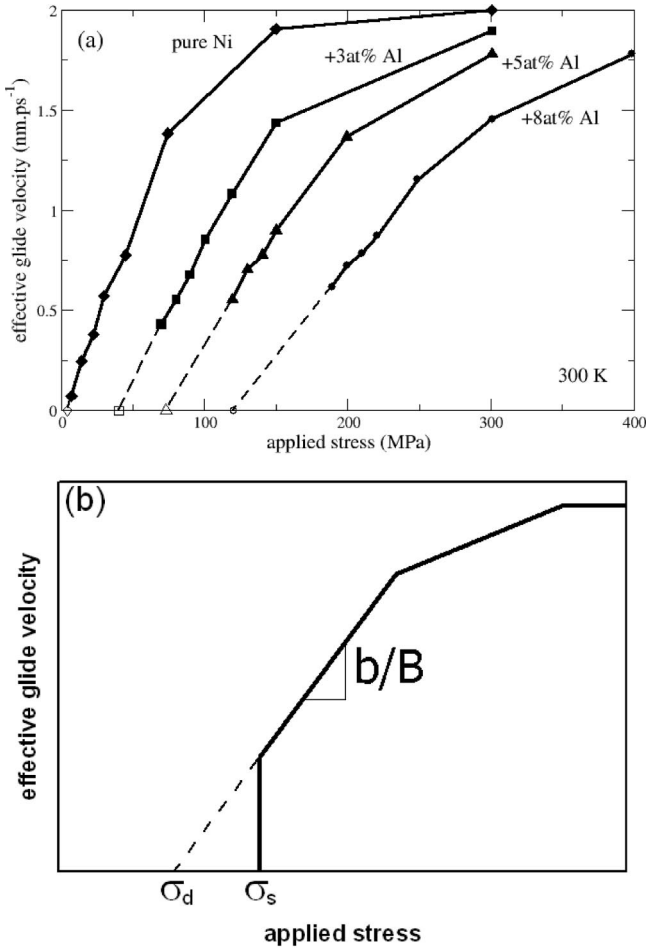

FIG. 4. (a) Effective glide velocity as a function of applied stress; (b) definition of the three parameters σ_s, σ_d, and B (see text).

300 K. The magnitude of the increase of σ_s with Al content compares well with reported values for the increase of the 0.2% elastic limit (10 to 20 MPa/at % Al), according to Ref. 34.

The temperature effect has not been studied in details. Preliminary results show that increasing the temperature from 300 to 500 K, in a random solid solution with 5 at % Al, results in a decrease of the *static* threshold from ~130 MPa to ~120 MPa; the *dynamical* threshold does not vary significantly, and the friction coefficient increases from ~20 to ~30 10^{-6} Pa.s.

C. Effect of the periodic boundary condition along the dislocation line

We found that *close to the static threshold*, the glide distance of the dislocation depends on the box size L_Y in the Y direction. Figure 6(a) shows the position of the dislocation as a function of time in a random solid solution with 3 at % Al under a shear stress of 65 MPa, for two distinct values of L_Y. As can be seen, for the smallest value of L_Y(17.3 nm), 65 MPa are not enough to produce sustained glide: The dislocation glides a fraction of the box length and stops (for at least 100 ps). With L_Y=21.56 nm and above, the glide distance is larger than four box lengths.

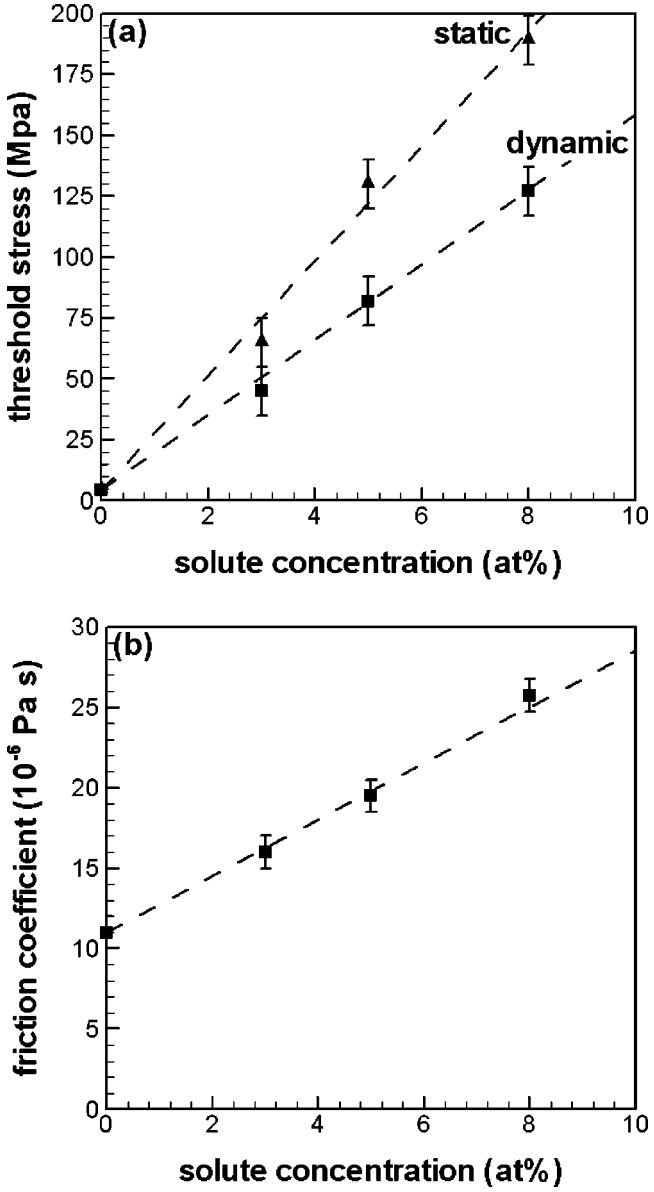

FIG. 5. Concentration dependence at 300 K of (a) the static (triangles) and dynamic (squares) threshold stresses, and (b) the friction coefficient per unit length.

A second effect of the value of L_Y is as follows. All the above simulations were performed with fully random solid solutions. Despite this randomness, it is found that, *close to the static threshold stress*, the glide distance of the dislocation depends on the seed of the random number generator used to construct the initial distribution of solute atoms. Figure 6(b) gives an example thereof; the effect is larger for smaller values of L_Y (compare the plain lines in Figs. 6(a) and 6(b). Notice that the very same simulations performed at 70 MPa with various L_Y values, exhibit extensive dislocation glide, while no glide at all ever occurs at 50 MPa. The value of the static threshold is thus defined within ±10 MPa.

Although a more detailed analysis is necessary to understand the effect of the box width, two possible origins may be proposed. Firstly, if the pinning centers are rare (less than one on a distance of L_y), the periodic boundary condition in

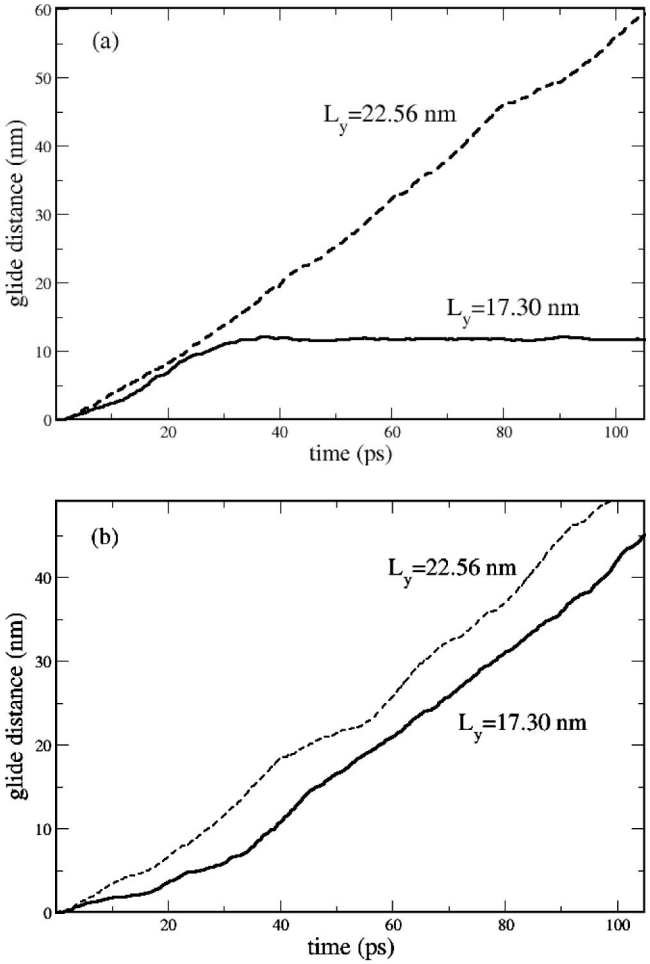

FIG. 6. Glide distance of the dislocation as a function of time in an ideal solid solution with 3 at % Al under 70 MPa; (a) for L_y = 17.3 nm (solid line) and L_y = 21.56 nm (dashed line) and the same seed of the random number generator for the initial configuration of the ideal solid; (b) same as (a) with another seed for the random number generator.

the Y direction imposes L_y as the distance between pinning centers: the larger L_y, i.e., the distance between pinning centers, and the lower the critical stress to escape. In addition, increasing L_y widens the range of available deformation modes for the dislocation line, which amounts to increase its flexibility, hence to decrease the effective line tension. Since, as will be shown below, the pinning centers are well separated and short ranged, an increased flexibility makes the depinning event easier, and the threshold stress lower. Also, as noticed, close to the static threshold stress, the smaller L_y, the more sensitive the glide distance to the initial configuration of the random solution: this suggests that the pinning centers only sample a small fraction of the Al atoms contained in the simulation cell.

IV. DISCUSSION

As seen on Fig. 3, the position of the dislocation segment as a function of time reveals a jerky glide motion. This suggests a "stop and go" type of analysis. Let us stress that we describe, here, the motion of the dislocation segment as a whole, as defined in Sec. IIC, not the change of shape of the dislocation and of the staking fault ribbon. Consider the position of the dislocation as a function of time, e.g., in a 3 at % random solid solution, at 300 K, under 70 MPa (Fig. 3). The time required to glide a distance of 300 nm is approximately 700 ps. The same curve can be analyzed at a finer scale: we may ask what is the time Δt required to glide a distance ΔX of 50, 20, or 10 nm. The time intervals Δt exhibit a complicated distribution, an example of which is given in Fig. 7. It contains information on the distribution of pinning strengths, which may be analyzed using a statistical approach. This work will be discussed in a future work.

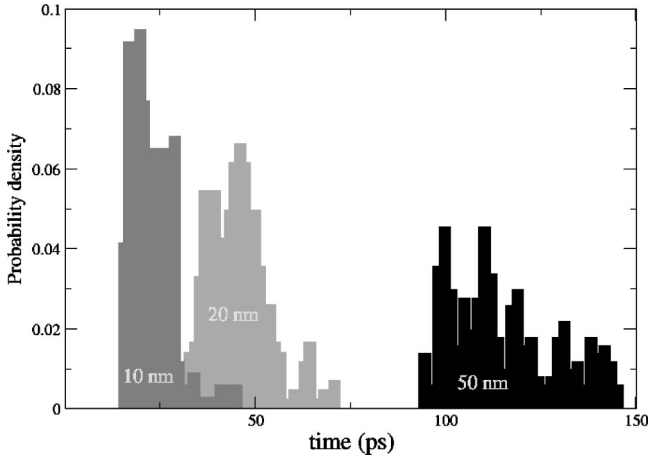

FIG. 7. Distribution of the time required to glide a distance ΔX (10, 20, 50 nm), in a random solid solution with 3 at % Al, under an applied stress of 70 MPa, at 300 K.

We now summarize our main findings, and outline a way of incorporating these results, obtained at the atomistic level, in a micromechanical model to describe the macroscopic plastic behavior.

The dislocation glide proceeds as follows:

— under large shear stresses, the dislocation glides smoothly at a velocity which saturates close to the shear wave speed;

— under lower stresses, the mean glide velocity is a linear function of the stress and extrapolates to zero at the dynamical threshold stress, σ_d;

— in the latter regime, a static threshold stress, σ_s, exists below which the dislocation stops for a "long" period of time after gliding "some" distance. Sustained macroscopic shear only occurs above σ_s.

An intuitive interpretation of the static and dynamic thresholds is as follows: The strong obstacles control the static threshold below which no long range dislocation motion is possible. Once these strong obstacles are overcome, the moving dislocation still feels from the weaker obstacles a pinning force, which slows down its motion. This is the physical origin of the dynamic threshold.

There is some arbitrariness in the definition of σ_s, since it depends on the value we choose for the observation time and for the minimum glide distance. We chose 300 nm for the minimum glide distance, since it guarantees that the disloca-

tion might propagate through a low forest density. We chose 50 ps as the observation time (i.e., maximum allowed waiting time) for computational reasons. We found, however, that within such a crude definition, the static threshold value is defined within ±10 MPa. Indeed a detailed study of the stress, temperature and composition dependence of the distribution of the waiting time would be of great interest[21] but the very large scatter of the waiting times at lower stresses, and their sensitivity to initial conditions, prevented us from making such a study.

Careful examination of the glide process at the atomic scale, revealed the following dislocation pinning mechanism: When a partial dislocation glides one step forward, it shifts the atoms above the glide plane with respect to those below the glide plane, by a vector $1/6\langle 112\rangle$. In the process of this displacement, some Al atoms (large compared to Ni atoms) are brought in close contact, a strongly repulsive configuration (this repulsion accounts for part of the stability of the $L1_2$ structure of Ni_3Al). On the contrary, if no such nearest neighbor Al-Al pair can ever form, the dislocation moves more easily. As an example, to test this idea, we generated a "constrained random" 8 at % Al solid solution, forbidding the shear induced formation of nearest neighbor Al-Al pairs around the glide plane: the way to achieve this, is to impose zero Al content in one of the two $(1\bar{1}1)$ planes across to the glide plane. Under 150 MPa, the glide velocity, in the constrained solution, is larger than in a fully random solution, as shown in Fig. 8(a). Similarly, glide is observed at 100 MPa, Fig. 8(b), much below the static threshold stress in the fully random solution (180 MPa).

We also studied the effect of the external stress on the glide velocity of the dislocation in a 3% solid solution constructed with the same constraint as above (Fig. 9), and compared with a fully, unconstrained, random solid solution. The Al-Al pairs across the glide plane are found to play an important role in the glide process. First they are, indeed, the obstacles, which determine the value of static threshold. Figure 9 clearly shows that in the absence of shear induced Al-Al pairs, the static threshold is much lower, close to its value in pure Ni. Second, when the external stress is much larger than the static threshold of the solid solution, the glide velocity is larger in the constrained solution (i.e., in the absence of shear induced Al-Al pairs) as compared to the unconstrained random solution: The shear induced Al-Al pairs form obstacles which slow down the dislocation glide and are responsible for the dynamic threshold stress.

This proves indeed that the origin of the chemical hardening process is the repulsive Al-Al interaction, and not the interaction between the Al atoms and the gliding dislocations. The waiting time on one of these obstacles would be controlled, we suggest, by the collective vibration of the few atoms the obstacle is made of.

The dependence with concentration of the static and the dynamic thresholds has been shown to be linear, in the range of concentrations investigated. This is indeed consistent with the fact that, if the dominant obstacles are solute pairs, their density scales as the square of the solute concentration and the elastic limit increases, according to Friedel statistics,[35,40] as the square root of the density of obstacles, i.e., as the solute concentration itself.[41]

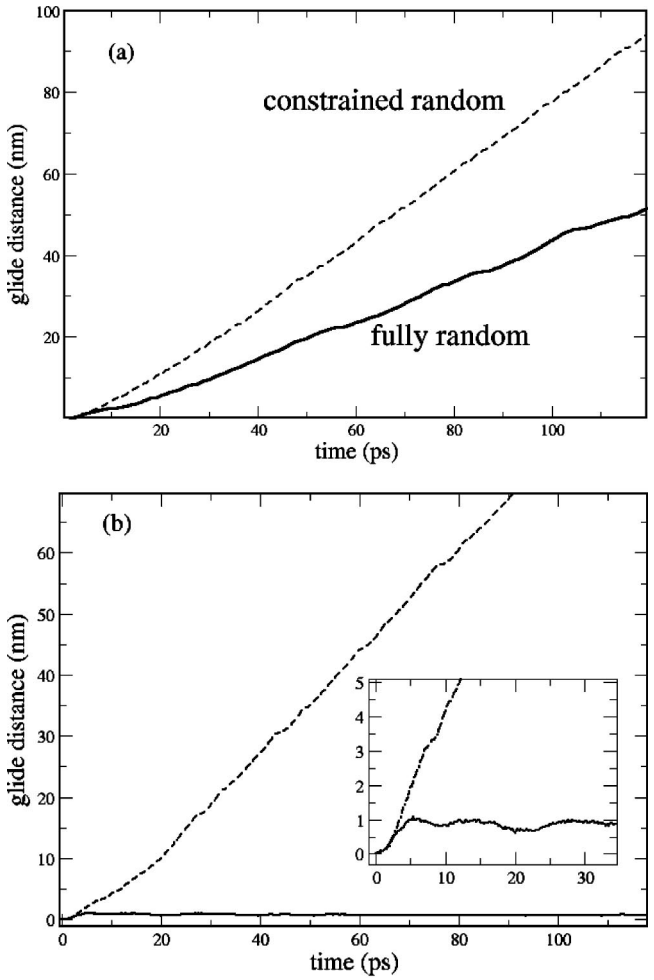

FIG. 8. (a) Glide distance of the dislocation as a function of time, under 150 MPa, in a 8 at % Al fully random solution, i.e., close to the static threshold stress (solid line) and for the same solution, constrained by removing Al atoms from one of the two $(1\bar{1}1)$ planes contiguous to the glide plane (dashed line). (b) Same as (a) for 100 MPa, i.e., much below the static threshold stress.

It is worth noticing that, in one of the very few systematic experimental studies of yield stress as function of solute content in a large range of composition, Wille *et al.*,[36] in Cu(Mn) solid solutions, reach the following conclusion: Using the standard theory of solute dislocation interaction to account for the observed hardening, the density of pinning centers is lower and their strength larger than expected for single solute pinning. They argue that MnMn doublets are responsible for the hardening.

The relevant quantity provided by our approach is the dislocation velocity for a given applied stress. It should be stressed that the dislocation velocities, which we generated, overlap the range accessible by experiments for similar applied stresses, despite the fact that the shear rates are several order of magnitude larger than experimental ones. The reason for this is the small size of the computational cell, which makes the dislocation density artificially large. In the spirit of multi-scale modeling, the quantity to be transferred from this study into larger scale models is the law for the glide velocity of a dislocation segment, i.e., Eq. (2), coupled with a

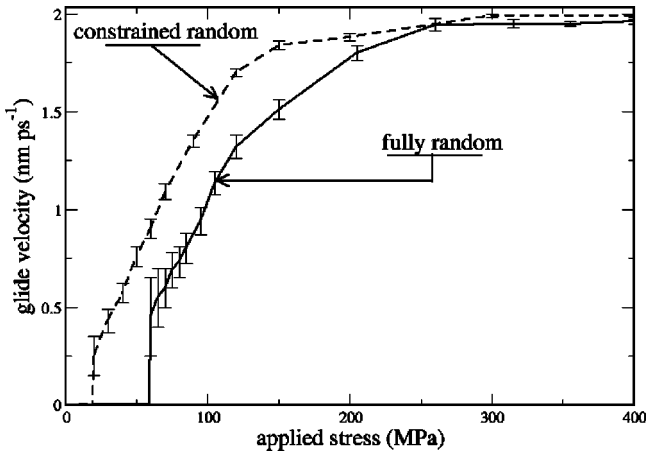

FIG. 9. Glide velocity as a function of the external stress, for a 3 at % solid solution with a fully random distribution of Al (solid line) and with a solute distribution, where one of the two $(\bar{1}11)$ planes contiguous to the glide plane, is constrained to be free of Al atoms (dashed line). The error bars are estimated by performing a sampling with respect to the seed of the random number generator used to construct the initial configuration of the solid solution.

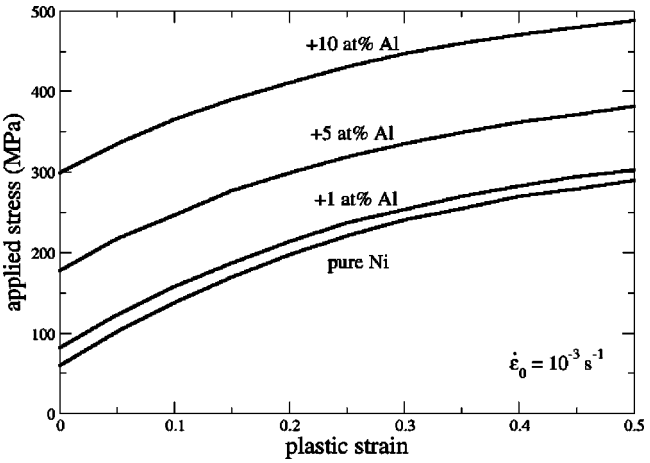

FIG. 10. Stress versus plastic strain as computed from the micromechanical model for 4 distinct Al contents: 0, 1, 5, 10 at %. The imposed strain rate is 10^{-3} s^{-1}; A=4.10^8 m^{-1}, D=6.5, α=0.3; the initial dislocation density is 10^{14} m^{-2}. The values of all the other parameters are taken from the present atomic scale simulation.

realistic description of the dislocation density.

In the following derivation, we have chosen the simplest classical evolution equation for the dislocation density to illustrate the feasibility of this approach. We do not claim that the macroscopic behavior is accurately described at this stage, since the present study deals only with the solute effects on dislocation glide. For instance, the present paper does not address the question of the solute effects on dynamic recovery.

Following Rodney *et al.*,[37] we take advantage of the shear rate as obtained from atomic scale simulations [Eq. (2)], to compute stress-strain curves as predicted by a simple micromechanical model. The rate of plastic shear, $\dot{\gamma}_p$ is given by Orowan's law:

$$\dot{\gamma}_p = \rho_d \, b \, V, \tag{3a}$$

and the dislocation density ρ_d changes in time because of the competition between multiplication and annihilation:[38]

$$\dot{\rho}_d = (A\sqrt{\rho_d} - D \, \rho_d)\dot{\gamma}_p. \tag{3b}$$

The first term in this equation describes the storage of dislocation on the so-called "forest dislocations," and the second terms accounts for the annihilation distance between dislocations of opposite sign. The parameter A is related to stage II hardening, and the parameter D is a measure of the efficiency of dynamic recovery. It is usually observed that A is independent of solute content, whereas D, which results from extra degrees of freedom such as cross slip or climb, depends on solute elements.[39] A quantitative description of the influence of solute elements on the stress strain curve would require a study of the effect of solutes on cross slip and climb, paralleling the one we have performed here for glide.

The dislocation velocity in Eq. (3a) is given by Eq. (2), except for the flow stress, which must now include the resistance opposed by the forest dislocations, on top of solute hardening depicted by σ_s. The spacing of obstacles responsible for solute hardening being much smaller that the spacing between forest dislocations, a linear superposition can be safely assumed:[40]

$$\sigma_y = \sigma_s + \alpha \, \mu b\sqrt{\rho_d}. \tag{3c}$$

The α parameter represents the pinning force of the forest dislocations.

The set of Eqs. (3a)–(3c) and (2) can be integrated with a given loading condition, namely a constant total strain rate test. Figure 10 shows typical stress-plastic strain curves computed with the values of the parameters as given by the present atomic scale simulation. The phenomenological parameters α, A, D introduced by the micromechanical model are given classical values.[37] The initial dislocation density is 10^{14} m^{-2}, and the imposed strain rate is 10^{-3} s^{-1}. As can be seen, the model qualitatively reproduces the increase of the flow stress with the solute content, but fails to reproduce the solute effect on the hardening which is observed, e.g., in Cu(Al) solid solutions. This is not a surprise, since the sensitivity of the parameter D to the solute content has been ignored.

V. CONCLUSION

Based on an EAM potential, which we have adapted, we have simulated the glide of an edge dislocation in random Ni(Al) solid solutions (1 to 8 at % Al) at 300 K. Within reasonable computer time, we could study the glide mechanism in the range of dislocation velocities of metallurgical interest.

Three parameters, σ_s, σ_d, and B, are found necessary to describe the rate of shear: σ_s is the static threshold stress,

below which the glide distance of the dislocation is not sufficient to insure sustained mesoscopic shearing; σ_d, is the dynamical threshold stress, which reflects the friction of the pinning potential on the moving dislocation; B, is the friction coefficient which relates the effective stress $(\sigma-\sigma_d)$ to the glide velocity. Both σ_s, σ_d, and B increase linearly with the solute content. Preliminary results suggest that σ_s decreases, and B increases with temperature, while σ_d remains unaffected.

The main conclusion of this study is that chemical hardening is not simply the result of a direct dislocation solute (*Al*) *interaction, but the result of close solute-solute* (*Al-Al*) *repulsion, when the passage of the dislocation forces them one against the other, which opposes the glide of one half crystal, with respect to the other*.

The qualitative analysis of the geometry of glide, as well as the preliminary results on the effect of temperature, suggest the need to revisit the concept of thermal activation of dislocation glide in solid solutions. The modification of the atomic position due to the moving dislocation, and its dependence with temperature have to be taken into account to develop a sound description of the thermally activated motion. The classical picture of the thermally activated motion of a dislocation in a potential computed with frozen atomic positions is likely to be of limited applicability when the solute concentration is such that the above described mechanism is mainly responsible for the hardening effect. In this spirit, the effect of short range order on dislocation motion deserves to be revisited.

Finally, we have outlined a method for integrating the present findings from the atomistic level into a micromechanical approach in order to predict macroscopic stress strain curves. While the increase of the yield stress with the composition is correctly described, an atomic scale study of cross slip and climb is needed to account for the influence of solute on dynamic recovery which controls further work hardening.

ACKNOWLEDGMENTS

Useful discussions and technical advice by Dr. E. Adam, Dr. J.L. Bocquet, Dr. D. Caillard, Dr. N.V. Doan, and Dr. M. Fivel are gratefully acknowledged, as well as enlightening comments by Professor. J. Friedel and Professor F.R. Nabarro. G.M. thanks Northwestern University (Department of Materials Science and Engineering) for hosting him as a visitor; part of this paper was written during this visit.

[1] V. Vitek, Cryst. Lattice Defects **5**, 1 (1974).
[2] C. Woodward and S. I. Rao, Philos. Mag. A **81**, 1305 & 1317 (2001); Phys. Rev. Lett. **88**, 216402 (2002).
[3] B. Legrand, Philos. Mag. A **52**, 83 (1985).
[4] D. Rodney and G. Martin, Phys. Rev. Lett. **82**, 3272 (1999).
[5] D. Rodney and G. Martin, Phys. Rev. B **61**, 8714 (2000).
[6] E. Kuramoto, J. Nucl. Mater. **276**, 143 (2000).
[7] B. D. Wirth, V. V. Bulatov, and T. Diaz de la Rubia, Mater. Res. Soc. Symp. Proc. **650**, 206 (2001); J. Eng. Mater. Technol. **124**, 329 (2002).
[8] Yu. N. Osetsky, D. J. Bacon, and V. Mohles, Philos. Mag. **83**, 3623 (2003).
[9] O. Rodriguez de la Fuente, J. A. Zimmerman, M. A. Gonzalez, J. de la Figuera, J. C. Hamilton, W. W. Pai, and J. M. Rojo, Phys. Rev. Lett. **88**, 036101 (2002).
[10] K. J. Van Vliet, J. Li, T. Zhu, S. Yip, and S. Suresh, Phys. Rev. B **67**, 104105 (2003).
[11] M. S. Daw and M. I. Baskes, Phys. Rev. Lett. **50**, 1285 (1983).
[12] S. J. Zhou, D. M. Beazley, P. S. Lomdahl, and B. L. Holian, Phys. Rev. Lett. **78**, 479 (1997).
[13] V. Bulatov, F. F. Abraham, L. Kubin, B. Devincre, and S. Yip, Nature (London) **391**, 669 (1998).
[14] P. Heino and E. Ristolainen, Nanostruct. Mater. **11**, 587 (1999).
[15] R. L. Fleisher, Acta Metall. **11**, 203 (1963); in *The Strengthening of Metals*, edited by D. Peckner (Reinold Press Edition, New York, 1964), p. 93.
[16] R. Labush, Phys. Status Solidi **41**, 659 (1970).
[17] P. Haasen, in *Dislocations in Solids*, edited by F. R. N. Nabarro (North-Holland, Amsterdam, 1979), Vol. 4, p. 155.
[18] R. J. Arsenault, S. Patu, and D. M. Esterling, Metall. Trans. A **20**, 1411 (1989).
[19] M. Dong, M. C. Marchetti, A. A. Middleton, and V. Vinokur, Phys. Rev. Lett. **70**, 662 (1993).
[20] H. G. Kaper, G. K. Leaf, D. M. Levine, and V. Vinokur, Phys. Rev. Lett. **71**, 3713 (1993).
[21] V. M. Vinokur, M. C. Marchetti, and L. W. Chen, Phys. Rev. Lett. **77**, 1845 (1996).
[22] G. D'Anna and W. Benoit, J. Appl. Phys. **82**, 5983 (1997).
[23] M. S. Daw, S. M. Foiles, and M. I. Baskes, Mater. Sci. Rep. **9**, 251 (1993).
[24] A. F. Voter and S. P. Chen, Mater. Res. Soc. Symp. Proc. **82**, 175 (1987).
[25] M. Ludwig and P. Gumbsch, Modell. Simul. Mater. Sci. Eng. **3**, 533 (1995).
[26] J. E. Angelo, N. R. Moody, and M. I. Baskes, Modell. Simul. Mater. Sci. Eng. **3**, 289 (1995).
[27] F. Ercolessi and J. B. Adams, Europhys. Lett. **26**, 583 (1994).
[28] F. Chassagne, M. Bessière, Y. Calvayrac, P. Cénédèse, and S. Lefèbvre, Acta Metall. **37**, 2329 (1989).
[29] E. S. Fisher, Scr. Metall. **20**, 279 (1986).
[30] E. Nembach and G. Neite, Prog. Mater. Sci. **29**, 177 (1985).
[31] P. Hansen, *Constitution of Binary Alloys* (McGraw Hill, New York, 1958).
[32] F. X. Kaiser and C. Stassis, Phys. Status Solidi A **64**, 335 (1981).
[33] R. Hultgren, P. D. Desai, D. T. Hawkins, M. Gleiser, and K. K. Kelley, *Selected values of thermodynamic properties of binary alloys* (ASM, Ohio, 1973).
[34] T. Shinoda, K. I. Masuda-Jindo, Y. Mishima, and T. Suzuki, Phys. Rev. B **35**, 2155 (1987).
[35] J. Friedel, *Dislocations* (Pergamon, New York, 1964).

[36] Th. Wille, G. Gieseke, and Ch. Schwink, Acta Metall. **35**, 2679 (1987).
[37] D. Rodney, G. Martin, and Y. Bréchet, Mater. Sci. Eng. A **309-310**, 198 (2001).
[38] U. F. Kocks, J. Eng. Mater. Technol. **98**, 76 (1976).
[39] U. F. Kocks and H. Mecking, Prog. Mater. Sci. **48**, 171 (2003).
[40] U. F Kocks, A. S. Argon, and M. S. Ashby, Prog. Mater. Sci. 19 (1975).
[41] We thank Pr. F. R. Nabarro for his suggestion.